arXiv:1004.4951

Observational Constraints on Cosmological Models with the Updated Long Gamma-Ray Bursts

Hao Wei *
Department of Physics, Beijing Institute of Technology, Beijing 100081, China

ABSTRACT

In the present work, by the help of the newly released Union2 compilation which consists of 557 Type Ia supernovae (SNIa), we calibrate 109 long Gamma-Ray Bursts (GRBs) with the well-known Amati relation, using the cosmology-independent calibration method proposed by Liang *et al.*. We have obtained 59 calibrated high-redshift GRBs which can be used to constrain cosmological models without the circularity problem (we call them "Hymnium" GRBs sample for convenience). Then, we consider the joint constraints on 7 cosmological models from the latest observational data, namely, the combination of 557 Union2 SNIa dataset, 59 calibrated Hymnium GRBs dataset (obtained in this work), the shift parameter R from the WMAP 7-year data, and the distance parameter A of the measurement of the baryon acoustic oscillation (BAO) peak in the distribution of SDSS luminous red galaxies. We also briefly consider the comparison of these 7 cosmological models.

PACS numbers: 98.80.Es, 95.36.+x, 98.70.Rz, 98.80.Cq

* email address: haowei@bit.edu.cn

I. INTRODUCTION

Since the discovery of current accelerated expansion of our universe [1], Type Ia supernovae (SNIa) have been considered to be a powerful probe to study this mysterious phenomenon. However, SNIa are plagued with extinction from the interstellar medium, and hence the current maximum redshift of SNIa is only about $z \simeq 1.755$. On the other hand, the redshift of the last scattering surface of cosmic microwave background (CMB) is about $z \simeq 1090$. There is a wide "desert" between the redshifts of SNIa and CMB. So, the observations at intermediate redshift are important to distinguish cosmological models.

Recently, Gamma-Ray Bursts (GRBs) have been proposed to be a complementary probe to SNIa (see e.g. [2] and references therein). So far, GRBs are the most intense explosions observed in our universe. Their high energy photons in the gamma-ray band are almost immune to dust extinction, in contrast to supernovae. Up to now, there are many GRBs observed at $0.1 < z \leq 8.1$, whereas the maximum redshift of GRBs is expected to be 10 or even larger [3]. Therefore, GRBs are considered to be a hopeful probe to fill the "desert" between the redshifts of SNIa and CMB. We refer to e.g. [2, 4–6] for some comprehensive reviews on the so-called GRB cosmology. As is well known, there is a circularity problem in the direct use of GRBs [7], mainly due to the lack of a set of low-redshift GRBs at $z < 0.1$ which are cosmology-independent. To alleviate the circularity problem, some statistical methods have been proposed, such as the scatter method [8], the luminosity distance method [8], and the Bayesian method [9]. Other methods trying to avoid the circularity problem have been proposed in e.g. [10, 11]. Recently, a new idea of the distance ladder to calibrate GRBs in a completely cosmology-independent manner has been proposed in [12, 13] independently. Similar to the case of calibrating SNIa as secondary standard candles by using Cepheid variables which are primary standard candles, we can also calibrate GRBs as standard candles with a large amount of SNIa. And then, the calibrated GRBs can be used to constrain cosmological models without the circularity problem. We refer to e.g. [12, 14, 15] for some relevant works.

It is worth noting that in the literature most relevant works mainly used the 69 GRBs compiled in [2] or the 70 GRBs compiled in [16]. As of the end of 2009, there are 109 long GRBs with measured redshift and spectral peak energy compiled in [17]. The number of usable GRBs is significantly increased [60]. Among these 109 GRBs, the data of 70 GRBs are taken from [16]; the data of 25 GRBs are taken from [18]; the data of remaining 14 GRBs (090516, 090618, 090715B, 090812, 090902B, 090926, 090926B, 091003, 091018, 091020, 091024, 091029, 091127, 091208B) are provided by L. Amati in private communication [19]. On the other hand, the cosmology-independent method to calibrate GRBs proposed in [12] needs a large amount of SNIa at $z < 1.4$. Thus, the SNIa dataset plays an important role in the calibration of GRBs. Previously, the relevant works (e.g. [12, 14, 15]) used the 192 Davis SNIa dataset or the 307 Union SNIa dataset to calibrate GRBs. Very recently, the Supernova Cosmology Project (SCP) collaboration released their Union2 compilation which consists of 557 SNIa [20]. The Union2 compilation is the largest published and spectroscopically confirmed SNIa sample to date. The number of usable SNIa is also significantly increased. Obviously, a larger SNIa dataset could bring a better interpolation for the cosmology-independent method to calibrate GRBs proposed in [12]. Motivated by both the significant improvements in GRBs and SNIa, in the present work, we update the calibration of GRBs with the well-known Amati relation, using the cosmology-independent method proposed in [12], and obtain 59 calibrated high-redshift GRBs which can be used to constrain cosmological models without the circularity problem (we call them "Hymnium" GRBs sample for convenience).

On the other hand, very recently the WMAP Collaboration also released their 7-year CMB data (WMAP7) in [21]. Therefore, it is natural to consider the joint constraints on cosmological models from these latest observational data, namely, the combination of 557 Union2 SNIa dataset [20], 59 calibrated Hymnium GRBs dataset (obtained in this work), the shift parameter R from the WMAP7 data [21], and the distance parameter A of the measurement of the BAO peak in the distribution of SDSS luminous red galaxies [22, 23]. In this work, we consider 7 cosmological models and obtain the observational constraints on them. Notice that we assume the universe to be spatially flat throughout this work.

This paper is organized as followings. In Sec. II, by the help of the newly released Union2 compilation which consists of 557 SNIa, we calibrate the 109 GRBs with Amati relation, using the cosmology-independent method proposed in [12]. In Sec. III, we briefly introduce the methodology to constrain cosmological models with the combined latest observational data. Then, we obtain the corresponding constraints on 7 cosmological models in Sec. IV. Further, we consider the comparison of these 7 models in Sec. V. Finally, we give the brief conclusions in Sec. VI.

II. UPDATING THE CALIBRATION OF GRBS WITH UNION2 SNIA DATA

In this section, as mentioned above, we are going to calibrate the 109 GRBs [17] (and [16, 18, 19]) by using the 557 Union2 SNIa data [20]. In fact, we are closely following the cosmology-independent calibration method used in [12, 15]. Notice that in the present work, we calibrate GRBs only with the Amati relation, so that we can use a larger GRBs dataset for single GRB luminosity relation. As in [12, 15], we choose $z = 1.4$ to be the divide line to separate GRBs into low- and high-redshift groups. In the 109 GRBs compiled by Amati [17] (and [16, 18, 19]), there are 50 GRBs at $z < 1.4$ and 59 GRBs at $z > 1.4$. The maximum redshift of these 109 GRBs is $z = 8.1$ for GRB 090423.

Several years ago, Amati *et al.* found the well-known $E_{\rm p,i} - E_{\rm iso}$ correlation in GRBs as $E_{\rm p,i} = K \times E_{\rm iso}^{m}$ by using 12 GRBs with known redshifts [24] (note that this correlation has been firstly discovered by Lloyd *et al.* [62] independently), where $E_{\rm p,i} = E_{\rm p,obs} \times (1+z)$ is the cosmological rest-frame spectral peak energy; the isotropic-equivalent radiated energy is given by

$$E_{\rm iso} = 4\pi\, d_L^2\, S_{\rm bolo}\, (1+z)^{-1}, \tag{1}$$

in which $S_{\rm bolo}$ is the bolometric fluence of gamma rays in the GRB at redshift z, and d_L is the luminosity distance of the GRB. Later, Amati *et al.* have updated it in [16–18, 25]. Up to now, some theoretical interpretations have been proposed for the Amati relation [4]. It might be geometrical effects due to the jet viewing angle with respect to a ring-shaped emission region [26], or with respect to a multiple sub-jet model structure [27]. An alternative explanation of the Amati relation is related to the dissipative mechanism responsible for the prompt emission [28]. However, we alert the readers to the fact that there is a considerable debate as to whether the Amati relation is an intrinsic effect or the result of detection biases (or a combination of these two) [63]. We refer to e.g. [61, 64] for some notable works which discuss the Amati relation in particular. They noted that many outliers are not included in the studies of Amati and Schaefer, and argued that this relation might simply be wrong, or its inferred scatter might be too low or different from the observed scatter [63]. Anyway, let us go ahead. For convenience, similar to [2], we can rewrite the Amati relation as

$$\log \frac{E_{\rm iso}}{\rm erg} = \lambda + b\, \log \frac{E_{\rm p,i}}{300\,{\rm keV}}\,, \tag{2}$$

where "log" indicates the logarithm to base 10, whereas λ and b are constants to be determined. In the literature, the Amati relation was calibrated with $E_{\rm iso}$ computed by *assuming* a ΛCDM cosmology with specified model parameters. As mentioned above, this is cosmology-dependent and the circularity problem follows. Here, we instead use the method proposed in [12] to calibrate the Amati relation in a cosmology-independent manner. We refer to the original paper [12] for more details.

Firstly, we derive the distance moduli for the 50 low-redshift ($z < 1.4$) GRBs of [17] (and [16, 18, 19]) by using cubic interpolation from the 557 Union2 SNIa compiled in [20]. We present the interpolated distance moduli μ of these 50 GRBs in the left panel of Fig. 1. The corresponding error bars are also plotted. In Table I, we give the numerical data of these 50 GRBs. As in [12], when the cubic interpolation is used, the error of the distance modulus μ for the GRB at redshift z can be calculated by

$$\sigma_\mu = \left(\sum_{i=1}^{4} A_i^2 \epsilon_{\mu,i}^2 \right)^{1/2}, \qquad \text{where} \qquad A_i \equiv \prod_{j \neq i} (z_j - z) \Big/ \prod_{j \neq i} (z_j - z_i)\,,$$

in which j runs from 1 to 4 but $j \neq i$; on the other hand, $\epsilon_{\mu,i}$ are the errors of the nearby SNIa whose redshifts are z_i. Then, using the well-known relation

$$\mu = 5 \log \frac{d_L}{\rm Mpc} + 25\,, \tag{3}$$

one can convert distance modulus μ into luminosity distance d_L (in units of Mpc). From Eq. (1) with the corresponding $S_{\rm bolo}$ given in [16, 18, 19], we can derive $E_{\rm iso}$ for these 50 GRBs at $z < 1.4$. We present them in the right panel of Fig. 1, whereas $E_{\rm p,i}$ for these 50 GRBs at $z < 1.4$ are taken from [16, 18, 19]. Also, we present the errors for these 50 GRBs at $z < 1.4$, by simply using the error propagation. From

Fig. 1, one can clearly see that the intrinsic scatter is dominating over the measurement errors. Therefore, as in [2, 12], the bisector of the two ordinary least squares [29] will be used. Following the procedure of the bisector of the two ordinary least squares described in [29], we find the best fit to be

$$b = 1.7828 \qquad \text{and} \qquad \lambda = 52.7838\,, \tag{4}$$

with 1σ uncertainties

$$\sigma_b = 0.0072 \qquad \text{and} \qquad \sigma_\lambda = 0.0041\,. \tag{5}$$

The best-fit calibration line Eq. (2) with b and λ in Eq. (4) is also plotted in the right panel of Fig. 1. From Eq. (5), it is easy to see that the calibration in this work is better than the one in [15].

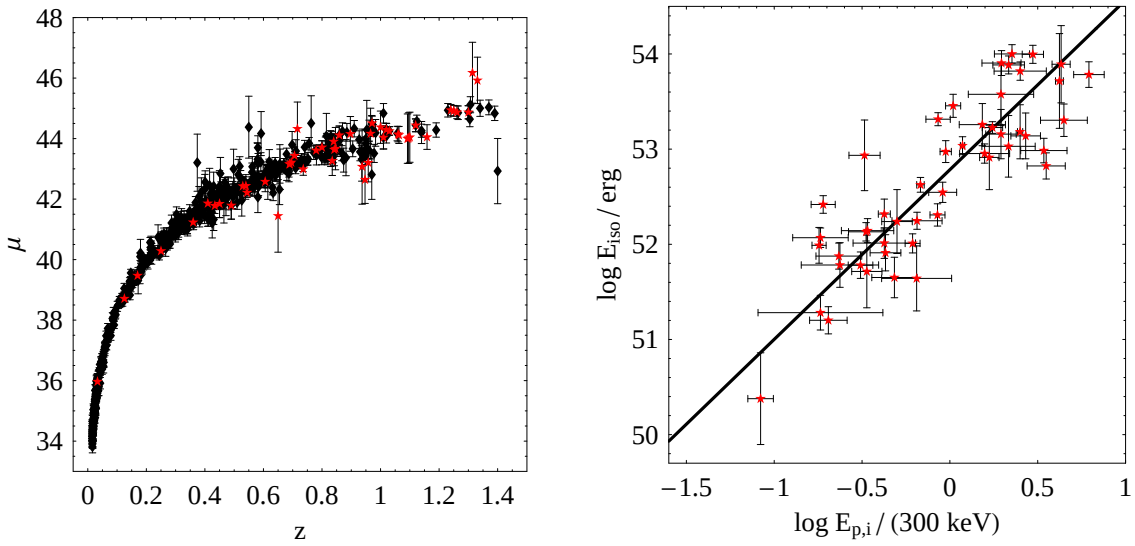

FIG. 1: Left panel: The Hubble diagram of 557 SNIa (black diamonds) and 50 low-redshift GRBs (red stars) whose distance moduli are derived by using cubic interpolation. Right panel: 50 GRBs data (red stars) in the $\log E_{\rm p,i}\,/(300\,{\rm keV}) - \log E_{\rm iso}\,/{\rm erg}$ plane. The best-fit calibration line is also plotted. See the text for details.

Next, we extend the calibrated Amati relation to high-redshift, namely $z > 1.4$. Since $E_{\rm p,i}$ for the 59 GRBs at $z > 1.4$ have been given in [16, 18, 19], we can derive $E_{\rm iso}$ from the calibrated Amati relation Eq. (2) with b and λ in Eq. (4). Then, we derive the distance moduli μ for these 59 GRBs at $z > 1.4$ using Eqs. (1) and (3) while their $S_{\rm bolo}$ can be taken from [16, 18, 19]. On the other hand, the propagated uncertainties are given by [2]

$$\sigma_\mu = \left[\left(\frac{5}{2}\sigma_{\log E_{\rm iso}}\right)^2 + \left(\frac{5}{2\ln 10}\,\frac{\sigma_{S_{\rm bolo}}}{S_{\rm bolo}}\right)^2\right]^{1/2}, \tag{6}$$

where

$$\sigma^2_{\log E_{\rm iso}} = \sigma^2_\lambda + \left(\sigma_b \log\frac{E_{\rm p,i}}{300\,{\rm keV}}\right)^2 + \left(\frac{b}{\ln 10}\,\frac{\sigma_{E_{\rm p,i}}}{E_{\rm p,i}}\right)^2 + \sigma^2_{E_{\rm iso,sys}}, \tag{7}$$

in which $\sigma_{E_{\rm iso,sys}}$ is the systematic error and it accounts the extra scatter of the luminosity relation. As in [2], by requiring the χ^2/dof of the 50 points at $z < 1.4$ in the $\log E_{\rm p,i}\,/(300\,{\rm keV}) - \log E_{\rm iso}\,/{\rm erg}$ plane about the best-fit calibration line to be unity, we find that

$$\sigma^2_{E_{\rm iso,sys}} = 0.1526. \tag{8}$$

Note that in principle $\sigma^2_{E_{\rm iso,sys}}$ is a free parameter. However, if we permit it to vary with cosmology, like in e.g. [65], there might be room for the circularity problem. Even one does not care this problem, the constraints on cosmological models become loose, mainly due to the fact that the number of free parameters has been increased. On the other hand, in the cosmology-independent calibration method proposed in [12], we have not used any cosmology when we calibrate GRBs at $z < 1.4$, unlike in [65] they calibrate all GRBs without using SNIa at low-redshift. Mainly due to the nature of the calibration method proposed in [12], we have no freedom to determine $\sigma^2_{E_{\rm iso,sys}}$ by cosmology, and hence we must use the method in [2] to fix it by requiring $\chi^2/dof = 1$. We admit that this prevents us to learn the systematics dominating the Amati relation. Nevertheless, we plot the derived distance moduli μ with 1σ uncertainties for these 59 GRBs at $z > 1.4$ in Fig. 2. We also present the numerical data of these 59 GRBs in Table II. For convenience, we call them "Hymnium" GRBs sample. It is worth noting that they are obtained in a completely cosmology-independent manner, and hence can be used to constrain cosmological models without the circularity problem.

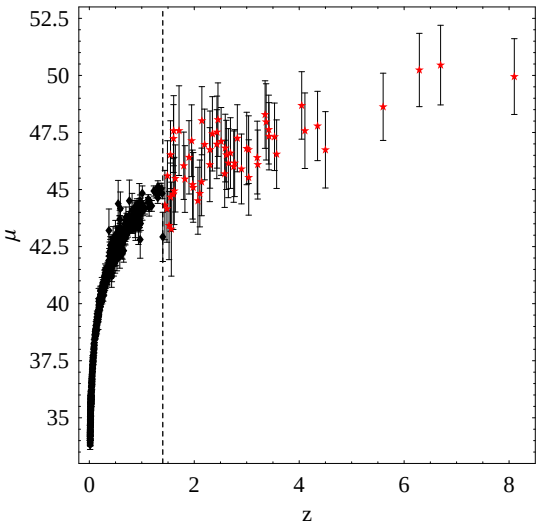

FIG. 2: The Hubble diagram of 557 Union2 SNIa (black diamonds) and 59 high-redshift Hymnium GRBs (red stars) whose distance moduli are derived by using the calibrated Amati relation. The dashed line indicates $z = 1.4$. See the text for details.

III. METHODOLOGY TO CONSTRAIN COSMOLOGICAL MODELS

Very recently, as mentioned in Sec. I, the SCP collaboration released their Union2 dataset which consists of 557 SNIa [20], whereas the WMAP Collaboration also released their 7-year CMB data (WMAP7) in [21]. On the other hand, as of the end of 2009, there are 109 long GRBs with measured redshift and spectral peak energy [17] (and [16, 18, 19]). The number of usable GRBs is significantly increased. Motivated by these significant updates in the observations of SNIa, CMB and GRBs, it is natural to consider the joint constraints on cosmological models with the latest observational data. Here, we use the combination of 557 Union2 SNIa dataset [20], 59 calibrated Hymnium GRBs dataset (obtained in this work, and whose numerical data are given in Table II), the shift parameter R from the WMAP7 data [21], and the distance parameter A of the measurement of the BAO peak in the distribution of SDSS luminous red galaxies [22, 23].

The data points of the 557 Union2 SNIa compiled in [20] and the 59 Hymnium GRBs dataset in Table II of this paper are given in terms of the distance modulus $\mu_{obs}(z_i)$. On the other hand, the theoretical distance modulus is defined as

$$\mu_{th}(z_i) \equiv 5\log_{10} D_L(z_i) + \mu_0 \,, \tag{9}$$

GRB	z	$S_{\rm bolo}$ (10^{-5} erg cm^{-2})	$E_{\rm p,i}$ (keV)	μ
060218	0.0331	2.20 ± 0.10	4.9 ± 0.3	35.97 ± 0.22
060614	0.125	5.90 ± 2.40	55 ± 45	38.71 ± 0.11
030329	0.17	21.50 ± 3.80	100 ± 23	39.47 ± 0.15
020903	0.25	0.016 ± 0.004	3.37 ± 1.79	40.29 ± 0.13
011121	0.36	24.30 ± 6.70	1060 ± 265	41.23 ± 0.17
020819B	0.41	1.60 ± 0.40	70 ± 21	41.86 ± 0.21
990712	0.434	1.40 ± 0.30	93 ± 15	41.78 ± 0.26
010921	0.45	1.80 ± 0.20	129 ± 26	41.85 ± 0.46
091127	0.49	2.34 ± 0.28	54 ± 5	41.79 ± 0.45
081007	0.5295	0.22 ± 0.041	61 ± 15	42.43 ± 0.29
090618	0.54	28.087 ± 3.37	257 ± 41	42.44 ± 0.11
090424	0.544	5.90 ± 1.15	273 ± 50	42.21 ± 0.16
050525A	0.606	2.60 ± 0.50	127 ± 10	42.58 ± 0.33
050416A	0.65	0.087 ± 0.009	25.1 ± 4.2	41.44 ± 1.20
080916	0.689	0.79 ± 0.079	184 ± 18	43.16 ± 0.23
020405	0.69	8.40 ± 0.70	354 ± 10	43.15 ± 0.22
970228	0.695	1.30 ± 0.10	195 ± 64	43.21 ± 0.21
991208	0.706	17.20 ± 1.40	313 ± 31	43.43 ± 0.29
041006	0.716	2.30 ± 0.60	98 ± 20	44.32 ± 0.88
090328	0.736	8.93 ± 2.061	1028 ± 312	42.99 ± 0.20
030528	0.78	1.40 ± 0.20	57 ± 9	43.61 ± 0.17
051022	0.8	32.60 ± 3.10	754 ± 258	43.71 ± 0.22
970508	0.835	0.34 ± 0.07	145 ± 43	43.26 ± 0.48
060814	0.84	3.80 ± 0.40	473 ± 155	43.90 ± 0.23
990705	0.842	9.80 ± 1.40	459 ± 139	43.63 ± 0.53
000210	0.846	8 ± 0.90	753 ± 26	43.67 ± 0.70
040924	0.859	0.49 ± 0.04	102 ± 35	44.11 ± 0.30
091003	0.8969	4.75 ± 0.79	810 ± 157	44.16 ± 0.57
080319B	0.937	49.70 ± 3.80	1261 ± 65	43.07 ± 1.24
071010B	0.947	0.74 ± 0.37	101 ± 20	42.64 ± 0.79
970828	0.958	12.30 ± 1.40	586 ± 117	43.20 ± 0.64
980703	0.966	2.90 ± 0.30	503 ± 64	44.17 ± 0.84
091018	0.971	0.30 ± 0.03	55 ± 20	44.51 ± 0.23
980326	1	0.18 ± 0.04	71 ± 36	44.38 ± 0.53
021211	1.01	0.42 ± 0.05	127 ± 52	44.04 ± 0.38
991216	1.02	24.80 ± 2.50	648 ± 134	44.29 ± 0.21
080411	1.03	5.70 ± 0.30	524 ± 70	44.25 ± 0.14
000911	1.06	23 ± 4.70	1856 ± 371	44.14 ± 0.25
091208B	1.063	0.79 ± 0.056	255 ± 25	44.12 ± 0.28
091024	1.092	16.57 ± 1.60	586 ± 251	44.00 ± 0.82
980613	1.096	0.19 ± 0.03	194 ± 89	44.02 ± 0.84
080413B	1.1	0.73 ± 0.092	150 ± 30	44.05 ± 0.83
000418	1.12	2.80 ± 0.50	284 ± 21	44.44 ± 0.21
061126	1.1588	8.70 ± 1.00	1337 ± 410	44.05 ± 0.41
090926B	1.24	0.83 ± 0.042	204 ± 10	44.94 ± 0.19
020813	1.25	16.30 ± 4.10	590 ± 151	44.92 ± 0.18
061007	1.261	21.10 ± 2.10	890 ± 124	44.87 ± 0.21
990506	1.3	21.70 ± 2.20	677 ± 156	44.87 ± 0.22
061121	1.314	5.10 ± 0.60	1289 ± 153	46.18 ± 1.01
071117	1.331	0.89 ± 0.21	647 ± 226	45.92 ± 0.77

TABLE I: The numerical data of 50 low-redshift GRBs at $z < 1.4$. The first 4 columns are taken from [16, 18, 19], whereas the last column is derived by using cubic interpolation from the 557 Union2 SNIa. These 50 low-redshift GRBs can be used to calibrate the Amati relation. See the text for details.

where $\mu_0 \equiv 42.38 - 5 \log_{10} h$ and h is the Hubble constant H_0 in units of 100 km/s/Mpc, whereas

$$D_L(z) = (1+z) \int_0^z \frac{d\tilde{z}}{E(\tilde{z}; \mathbf{p})} \,, \tag{10}$$

in which $E \equiv H/H_0$, and $\mathbf{p}$ denotes the model parameters. Correspondingly, the χ^2 from the 557 Union2

SNIa and the 59 Hymnium GRBs is given by

$$\chi^2_\mu(\mathbf{p}) = \sum_i \frac{\left[\mu_{obs}(z_i) - \mu_{th}(z_i)\right]^2}{\sigma^2(z_i)}\,, \tag{11}$$

where σ is the corresponding 1σ error. The parameter μ_0 is a nuisance parameter but it is independent of the data points. One can perform an uniform marginalization over μ_0. However, there is an alternative way. Following [30, 31], the minimization with respect to μ_0 can be made by expanding the χ^2_μ of Eq. (11) with respect to μ_0 as

$$\chi^2_\mu(\mathbf{p}) = \tilde{A} - 2\mu_0\tilde{B} + \mu_0^2\tilde{C}\,, \tag{12}$$

where

$$\tilde{A}(\mathbf{p}) = \sum_i \frac{\left[\mu_{obs}(z_i) - \mu_{th}(z_i;\mu_0=0,\mathbf{p})\right]^2}{\sigma^2_{\mu_{obs}}(z_i)}\,,$$

$$\tilde{B}(\mathbf{p}) = \sum_i \frac{\mu_{obs}(z_i) - \mu_{th}(z_i;\mu_0=0,\mathbf{p})}{\sigma^2_{\mu_{obs}}(z_i)}\,, \qquad \tilde{C} = \sum_i \frac{1}{\sigma^2_{\mu_{obs}}(z_i)}\,.$$

Eq. (12) has a minimum for $\mu_0 = \tilde{B}/\tilde{C}$ at

$$\tilde{\chi}^2_\mu(\mathbf{p}) = \tilde{A}(\mathbf{p}) - \frac{\tilde{B}(\mathbf{p})^2}{\tilde{C}}\,. \tag{13}$$

Since $\chi^2_{\mu,\,min} = \tilde{\chi}^2_{\mu,\,min}$ obviously, we can instead minimize $\tilde{\chi}^2_\mu$ which is independent of μ_0. In fact, by this method, we have just marginalized over μ_0 analytically, and then simplified our computing.

There are some other observational data relevant to this work, such as the observations of CMB anisotropy [21] and large-scale structure (LSS) [22, 23]. However, using the full data of CMB and LSS to perform a global fitting consumes a large amount of time and power. As an alternative, one can instead use the shift parameter R from the CMB, and the distance parameter A of the measurement of the baryon acoustic oscillation (BAO) peak in the distribution of SDSS luminous red galaxies. In the literature, the shift parameter R and the distance parameter A have been used extensively. It is argued that they are model-independent [32], while R and A contain the main information of the observations of CMB and BAO, respectively. As is well known, the shift parameter R of the CMB is defined by [32, 33]

$$R \equiv \Omega_{m0}^{1/2}\int_0^{z_*}\frac{d\tilde{z}}{E(\tilde{z})}\,, \tag{14}$$

where Ω_{m0} is the present fractional density of pressureless matter; the redshift of recombination $z_* = 1091.3$ which has been updated in the WMAP7 data [21]. The shift parameter R relates the angular diameter distance to the last scattering surface, the comoving size of the sound horizon at z_* and the angular scale of the first acoustic peak in CMB power spectrum of temperature fluctuations [32, 33]. The value of R has been updated to 1.725 ± 0.018 from the WMAP7 data [21]. On the other hand, the distance parameter A of the measurement of the BAO peak in the distribution of SDSS luminous red galaxies [22] is given by

$$A \equiv \Omega_{m0}^{1/2}E(z_b)^{-1/3}\left[\frac{1}{z_b}\int_0^{z_b}\frac{d\tilde{z}}{E(\tilde{z})}\right]^{2/3}\,, \tag{15}$$

where $z_b = 0.35$. In [23], the value of A has been determined to be $0.469\,(n_s/0.98)^{-0.35} \pm 0.017$. Here the scalar spectral index n_s is taken to be 0.963, which has been updated from the WMAP7 data [21]. So, the total χ^2 is given by

$$\chi^2 = \tilde{\chi}^2_\mu + \chi^2_{CMB} + \chi^2_{BAO}\,, \tag{16}$$

where $\tilde{\chi}^2_\mu$ is given in Eq. (13), $\chi^2_{CMB} = (R - R_{obs})^2/\sigma_R^2$ and $\chi^2_{BAO} = (A - A_{obs})^2/\sigma_A^2$. The best-fit model parameters are determined by minimizing the total χ^2. As in [34, 66], the 68% confidence level is determined by $\Delta\chi^2 \equiv \chi^2 - \chi^2_{min} \leq 1.0$, 2.3 and 3.53 for $n_p = 1$, 2 and 3, respectively, where n_p is the number of free model parameters. On the other hand, the 95% confidence level is determined by $\Delta\chi^2 \equiv \chi^2 - \chi^2_{min} \leq 4.0$, 6.17 and 8.02 for $n_p = 1$, 2 and 3, respectively.

GRB	z	$S_{\rm bolo}$ (10^{-5} erg cm^{-2})	$E_{\rm p,i}$ (keV)	μ
050318	1.44	0.42 ± 0.03	115 ± 25	44.32 ± 1.52
010222	1.48	14.60 ± 1.50	766 ± 30	44.15 ± 1.46
060418	1.489	2.30 ± 0.50	572 ± 143	45.60 ± 1.54
030328	1.52	6.40 ± 0.60	328 ± 55	43.43 ± 1.50
070125	1.547	13.30 ± 1.30	934 ± 148	44.67 ± 1.49
090102	1.547	3.48 ± 0.63	1149 ± 166	46.53 ± 1.49
040912	1.563	0.21 ± 0.06	44 ± 33	43.27 ± 2.06
990123	1.6	35.80 ± 5.80	1724 ± 466	44.80 ± 1.55
071003	1.604	5.32 ± 0.59	2077 ± 286	47.23 ± 1.48
090418	1.608	2.35 ± 0.59	1567 ± 384	47.58 ± 1.54
990510	1.619	2.60 ± 0.40	423 ± 42	44.94 ± 1.47
080605	1.6398	3.40 ± 0.28	650 ± 55	45.49 ± 1.47
091020	1.71	0.11 ± 0.034	280 ± 190	47.58 ± 1.96
080514B	1.8	2.027 ± 0.48	627 ± 65	46.04 ± 1.47
090902B	1.822	32.38 ± 1.01	2187 ± 31	45.46 ± 1.46
020127	1.9	0.38 ± 0.01	290 ± 100	46.41 ± 1.61
080319C	1.95	1.50 ± 0.30	906 ± 272	47.14 ± 1.57
081008	1.9685	0.96 ± 0.09	261 ± 52	45.22 ± 1.51
030226	1.98	1.30 ± 0.10	289 ± 66	45.09 ± 1.53
000926	2.07	2.60 ± 0.60	310 ± 20	44.51 ± 1.47
090926	2.1062	15.08 ± 0.77	974 ± 50	44.83 ± 1.46
011211	2.14	0.50 ± 0.06	186 ± 24	45.33 ± 1.48
071020	2.145	0.87 ± 0.40	1013 ± 160	48.015 ± 1.49
050922C	2.198	0.47 ± 0.16	415 ± 111	46.97 ± 1.55
060124	2.296	3.40 ± 0.50	784 ± 285	46.09 ± 1.62
021004	2.3	0.27 ± 0.04	266 ± 117	46.75 ± 1.69
051109A	2.346	0.51 ± 0.05	539 ± 200	47.44 ± 1.63
060908	2.43	0.73 ± 0.07	514 ± 102	46.99 ± 1.51
080413	2.433	0.56 ± 0.14	584 ± 180	47.52 ± 1.58
090812	2.452	3.077 ± 0.53	2000 ± 700	48.06 ± 1.61
081121	2.512	1.71 ± 0.33	871 ± 123	47.11 ± 1.49
081118	2.58	0.27 ± 0.057	147 ± 14	45.69 ± 1.47
080721	2.591	7.86 ± 1.37	1741 ± 227	46.82 ± 1.48
050820	2.612	6.40 ± 0.50	1325 ± 277	46.52 ± 1.52
030429	2.65	0.14 ± 0.02	128 ± 26	46.16 ± 1.51
080603B	2.69	0.64 ± 0.058	376 ± 100	46.60 ± 1.55
091029	2.752	0.47 ± 0.044	230 ± 66	46.00 ± 1.56
081222	2.77	1.67 ± 0.17	505 ± 34	46.16 ± 1.47
050603	2.821	3.50 ± 0.20	1333 ± 107	47.25 ± 1.47
050401	2.9	1.90 ± 0.40	467 ± 110	45.90 ± 1.53
090715B	3	1.09 ± 0.17	536 ± 172	46.80 ± 1.59
080607	3.036	8.96 ± 0.48	1691 ± 226	46.75 ± 1.48
081028	3.038	0.81 ± 0.095	234 ± 93	45.53 ± 1.65
020124	3.2	1.20 ± 0.10	448 ± 148	46.40 ± 1.59
060526	3.21	0.12 ± 0.06	105 ± 21	46.095 ± 1.51
080810	3.35	1.82 ± 0.20	1470 ± 180	48.28 ± 1.48
030323	3.37	0.12 ± 0.04	270 ± 113	47.96 ± 1.67
971214	3.42	0.87 ± 0.11	685 ± 133	47.63 ± 1.51
060707	3.425	0.23 ± 0.04	279 ± 28	47.33 ± 1.47
060115	3.53	0.25 ± 0.04	285 ± 34	47.31 ± 1.48
090323	3.57	14.98 ± 1.83	1901 ± 343	46.55 ± 1.50
060206	4.048	0.14 ± 0.03	394 ± 46	48.68 ± 1.48
090516	4.109	1.96 ± 0.38	971 ± 390	47.58 ± 1.65
080916C	4.35	10.13 ± 2.13	2646 ± 566	47.79 ± 1.52
000131	4.5	4.70 ± 0.80	987 ± 416	46.74 ± 1.67
060927	5.6	0.27 ± 0.04	475 ± 47	48.62 ± 1.47
050904	6.29	2 ± 0.20	3178 ± 1094	50.24 ± 1.61
080913	6.695	0.12 ± 0.035	710 ± 350	50.45 ± 1.74
090423	8.1	0.12 ± 0.032	491 ± 200	49.95 ± 1.66

TABLE II: The numerical data of 59 calibrated GRBs at $z > 1.4$. The first 4 columns are taken from [16, 18, 19], whereas the last column is derived by using the calibrated Amati relation. These 59 calibrated GRBs are called Hymnium sample, and can be used to constrain cosmological models without the circularity problem.

IV. OBSERVATIONAL CONSTRAINTS ON COSMOLOGICAL MODELS

A. Parameterized models

1. ΛCDM model

As is well known, for the ΛCDM model,

$$E(z) = \sqrt{\Omega_{m0}(1+z)^3 + (1-\Omega_{m0})}\,. \tag{17}$$

It is easy to obtain the total χ^2 as a function of the single model parameter Ω_{m0} for the ΛCDM model. We present the corresponding χ^2 and likelihood $\mathcal{L} \propto e^{-\chi^2/2}$ in Fig. 3. The best fit has $\chi^2_{min} = 566.173$, whereas the best-fit parameter is $\Omega_{m0} = 0.2706^{+0.0138}_{-0.0134}$ (with 1σ uncertainty) $^{+0.0282}_{-0.0263}$ (with 2σ uncertainty).

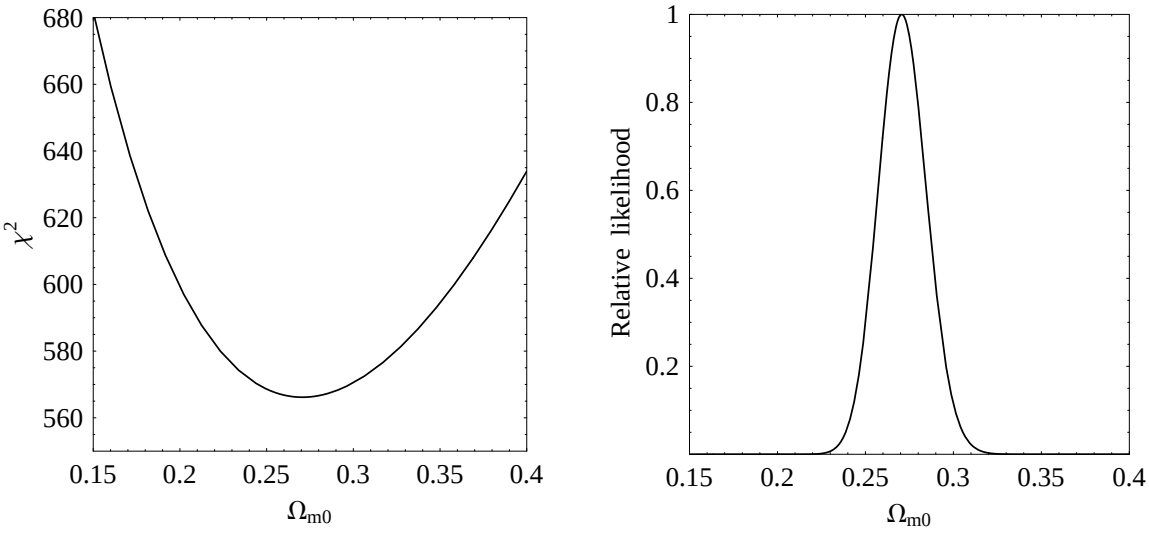

FIG. 3: The χ^2 and likelihood $\mathcal{L} \propto e^{-\chi^2/2}$ as functions of Ω_{m0} for the ΛCDM model.

2. XCDM model

Next, we consider the XCDM model. It is also well known that in the spatially flat universe which contains pressureless matter and dark energy whose equation-of-state parameter (EoS) is a constant w_x, the corresponding $E(z)$ is given by

$$E(z) = \sqrt{\Omega_{m0}(1+z)^3 + (1-\Omega_{m0})(1+z)^{3(1+w_x)}}\,. \tag{18}$$

By minimizing the corresponding total χ^2 in Eq. (16), we find the best-fit parameters $\Omega_{m0} = 0.2704$ and $w_x = -0.9967$, while $\chi^2_{min} = 566.168$. In Fig. 4, we present the corresponding 68% and 95% confidence level contours in the $\Omega_{m0} - w_x$ parameter space for the XCDM model.

3. CPL model

Here, we consider the familiar Chevallier-Polarski-Linder (CPL) model [35], in which the EoS of dark energy is parameterized as

$$w_{de} = w_0 + w_a(1-a) = w_0 + w_a\frac{z}{1+z}\,, \tag{19}$$

where w_0 and w_a are constants. As is well known, the corresponding $E(z)$ is given by [34, 36, 37]

$$E(z)=\left[\Omega_{m0}(1+z)^3+(1-\Omega_{m0})\,(1+z)^{3(1+w_0+w_a)}\exp\left(-\frac{3w_a z}{1+z}\right)\right]^{1/2}. \tag{20}$$

There are 3 independent parameters in this model. By minimizing the corresponding total χ^2 in Eq. (16), we find the best-fit parameters $\Omega_{m0}=0.2719$, $w_0=-1.0451$ and $w_a=0.2635$, while $\chi^2_{min}=566.007$. In Fig. 5, we present the corresponding 68% and 95% confidence level contours in the w_0-w_a plane for the CPL model. Also, the 68% and 95% confidence level contours in the $\Omega_{m0}-w_0$ plane and the $\Omega_{m0}-w_a$ plane for the CPL model are shown in Fig. 6.

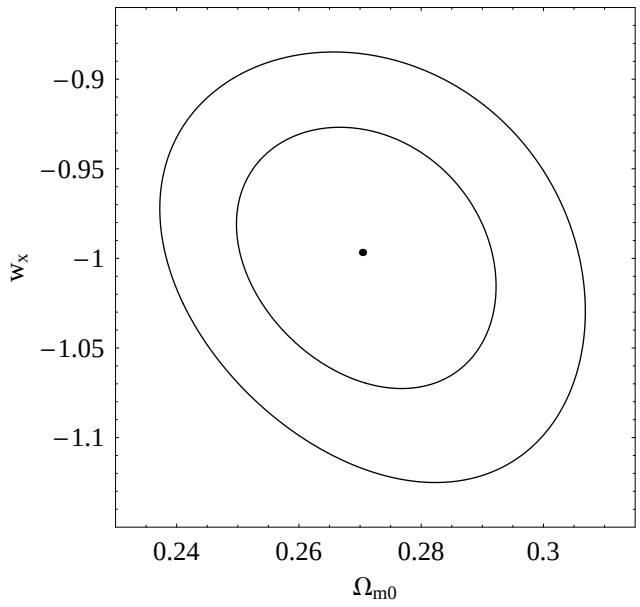

FIG. 4: The 68% and 95% confidence level contours in the $\Omega_{m0}-w_X$ parameter space for the XCDM model. The best-fit parameters are also indicated by a black solid point.

B. DGP model

One of the simplest modified gravity models is the so-called Dvali-Gabadadze-Porrati (DGP) braneworld model [38, 39], which entails altering the Einstein-Hilbert action by a term arising from large extra dimensions. For a list of references on the DGP model, see e.g. [40, 41] and references therein. As is well known, for the spatially flat DGP model (here we only consider the self-accelerating branch), $E(z)$ is given by [39–41]

$$E(z)=\sqrt{\Omega_{m0}(1+z)^3+\Omega_{rc}}+\sqrt{\Omega_{rc}}\,, \tag{21}$$

where Ω_{rc} is a constant. It is easy to see that $E(z=0)=1$ requires

$$\Omega_{m0}=1-2\sqrt{\Omega_{rc}}\,. \tag{22}$$

Therefore, the DGP model has only one independent model parameter Ω_{rc}. Notice that $0\leq\Omega_{rc}\leq 1/4$ is required by $0\leq\Omega_{m0}\leq 1$. It is easy to obtain the total χ^2 as a function of the single model parameter Ω_{rc}. In Fig. 7, we plot the corresponding χ^2 and likelihood $\mathcal{L}\propto e^{-\chi^2/2}$. The best fit has $\chi^2_{min}=611.794$, whereas the best-fit parameter is $\Omega_{rc}=0.1356^{+0.0048}_{-0.0049}$ (with 1σ uncertainty) $^{+0.0095}_{-0.0099}$ (with 2σ uncertainty).

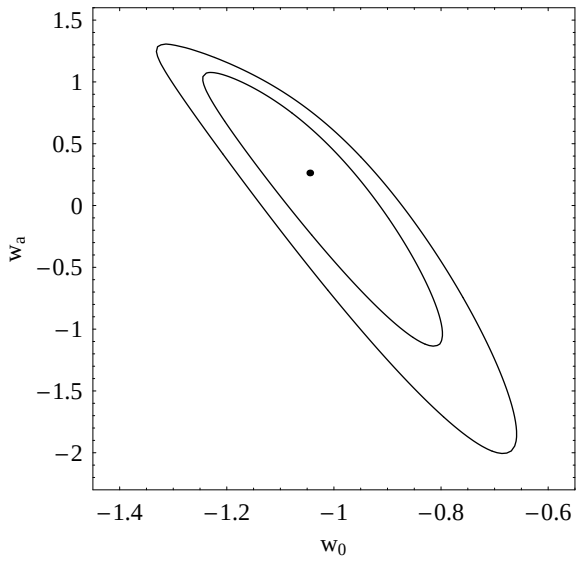

FIG. 5: The 68% and 95% confidence level contours in the $w_0 - w_a$ plane for the CPL model. The best-fit parameters are also indicated by a black solid point.

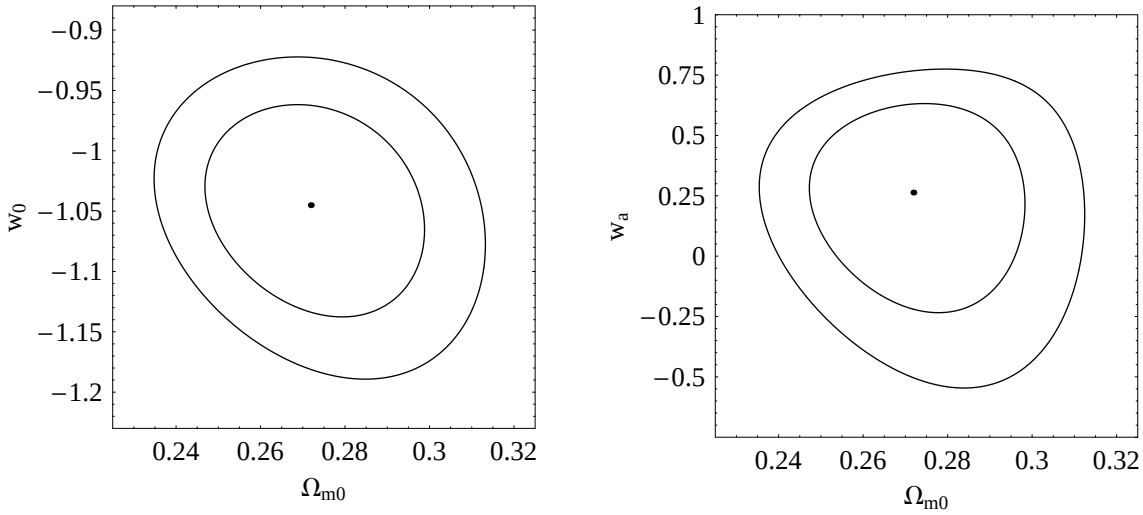

FIG. 6: The same as in Fig. 5, except for the $\Omega_{m0} - w_0$ plane and the $\Omega_{m0} - w_a$ plane.

C. New agegraphic dark energy model

In [42, 43], the so-called new agegraphic dark energy (NADE) model has been proposed recently, based on the Károlyházy uncertainty relation which arises from quantum mechanics together with general relativity. In this model, the energy density of NADE is given by [42, 43]

$$\rho_q = \frac{3n^2 m_p^2}{\eta^2}\,, \tag{23}$$

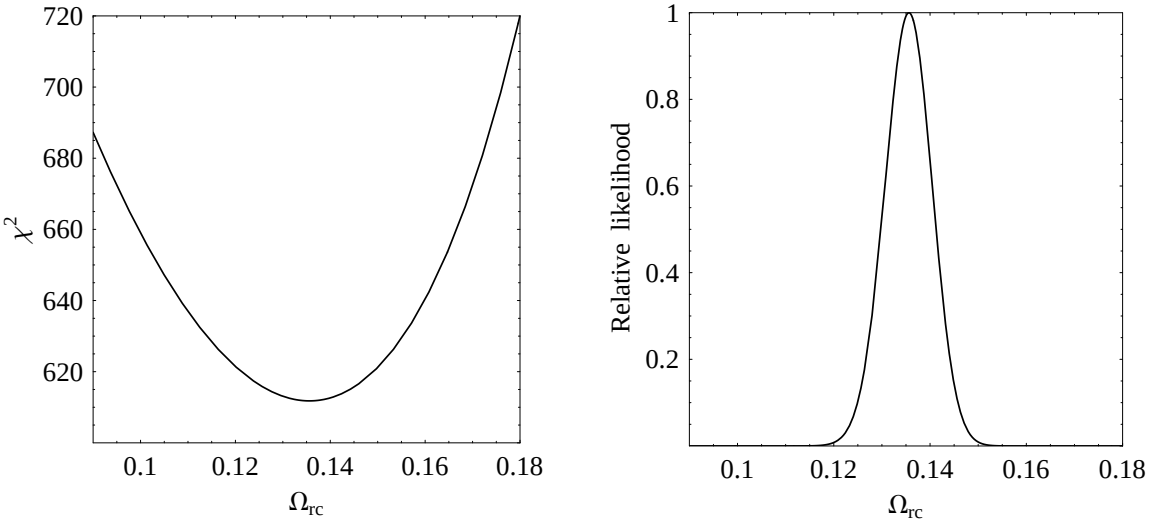

FIG. 7: The χ^2 and likelihood $\mathcal{L} \propto e^{-\chi^2/2}$ as functions of Ω_{rc} for the DGP model.

where m_p is the reduced Planck mass; n is a constant of order unity; η is the conformal time

$$\eta \equiv \int \frac{dt}{a} = \int \frac{da}{a^2 H}\,, \tag{24}$$

in which $a = (1+z)^{-1}$ is the scale factor. Obviously, $\dot{\eta} = 1/a$, where a dot denotes the derivative with respect to cosmic time t. The corresponding fractional energy density of NADE reads

$$\Omega_q \equiv \frac{\rho_q}{3m_p^2 H^2} = \frac{n^2}{H^2\eta^2}\,. \tag{25}$$

From the Friedmann equation $H^2 = (\rho_m + \rho_q)\,/\left(3m_p^2\right)$, the energy conservation equation $\dot{\rho}_m + 3H\rho_m = 0$, and Eqs. (23)—(25), we find that the equation of motion for Ω_q is given by [42, 43]

$$\frac{d\Omega_q}{dz} = -\Omega_q\,(1-\Omega_q)\left[3(1+z)^{-1} - \frac{2}{n}\sqrt{\Omega_q}\right]. \tag{26}$$

From the energy conservation equation $\dot{\rho}_q + 3H(\rho_q + p_q) = 0$, and Eqs. (23)—(25), it is easy to find that the EoS of NADE is given by [42, 43]

$$w_q \equiv \frac{p_q}{\rho_q} = -1 + \frac{2}{3n}\frac{\sqrt{\Omega_q}}{a}\,. \tag{27}$$

When $a \to \infty$, $\Omega_q \to 1$, thus $w_q \to -1$ in the late time. When $a \to 0$, $\Omega_q \to 0$, so $0/0$ appears in w_q and hence we cannot directly obtain w_q from Eq. (27). Let us consider the matter-dominated epoch, in which $H^2 \propto \rho_m \propto a^{-3}$. Thus, $a^{1/2}da \propto dt = ad\eta$. Then, we have $\eta \propto a^{1/2}$. From Eq. (23), $\rho_q \propto a^{-1}$. From the energy conservation equation $\dot{\rho}_q + 3H\rho_q(1+w_q) = 0$, we obtain $w_q = -2/3$ in the matter-dominated epoch. Since $\rho_m \propto a^{-3}$ and $\rho_q \propto a^{-1}$, it is expected that $\Omega_q \propto a^2$. Comparing $w_q = -2/3$ with Eq. (27), we find that $\Omega_q = n^2a^2/4$ in the matter-dominated epoch as expected. For $a \ll 1$, provided that n is of order unity, $\Omega_q \ll 1$ naturally follows. There are many interesting features in the NADE model and we refer to the original papers [42, 43] for more details.

At first glance, one might consider that NADE is a two-parameter model. However, as shown in [42], NADE is a *single-parameter* model in practice, thanks to its special analytic feature $\Omega_q = n^2a^2/4 =$

$n^2(1+z)^{-2}/4$ in the matter-dominated epoch, as mentioned above. If n is given, we can obtain $\Omega_q(z)$ from Eq. (26) with the initial condition $\Omega_q(z_{ini}) = n^2(1+z_{ini})^{-2}/4$ at any z_{ini} which is deep enough into the matter-dominated epoch (we choose $z_{ini} = 2000$ as in [42]), instead of $\Omega_q(z=0) = 1-\Omega_{m0}$ at $z = 0$. Then, all other physical quantities, such as $\Omega_m(z) = 1-\Omega_q(z)$ and $w_q(z)$ in Eq. (27), can be obtained correspondingly. So, $\Omega_{m0} = \Omega_m(z=0)$, $\Omega_{q0} = \Omega_q(z=0)$ and $w_{q0} = w_q(z=0)$ are *not* independent model parameters. The only free model parameter is n. Therefore, the NADE model is a *single-parameter* model in practice.

From the Friedmann equation $H^2 = (\rho_m + \rho_q) \,/\, \left(3m_p^2\right)$, we have

$$E(z) = \left[\frac{\Omega_{m0}(1+z)^3}{1-\Omega_q(z)}\right]^{1/2}. \tag{28}$$

If the single model parameter n is given, we can obtain $\Omega_q(z)$ from Eq. (26). Thus, we get $\Omega_{m0} = 1-\Omega_q(z=0)$. So, $E(z)$ is at hand. Therefore, we can find the corresponding total χ^2 in Eq. (16). In Fig. 8, we plot the total χ^2 and likelihood $\mathcal{L} \propto e^{-\chi^2/2}$ as functions of n. The best fit has $\chi^2_{min} = 594.449$, whereas the best-fit parameter is $n = 2.8865^{+0.0832}_{-0.0818}$ (with 1σ uncertainty) $^{+0.1680}_{-0.1622}$ (with 2σ uncertainty).

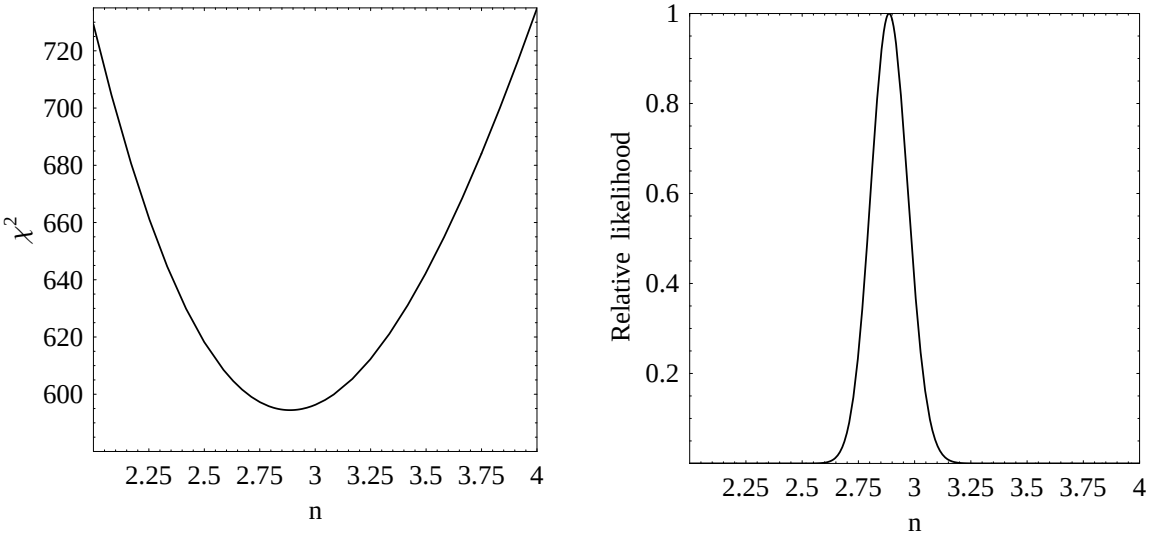

FIG. 8: The χ^2 and likelihood $\mathcal{L} \propto e^{-\chi^2/2}$ as functions of n for the NADE model.

D. Holographic dark energy model

The so-called holographic dark energy (HDE) has been studied extensively in the literature. It is proposed from the holographic principle [44, 45] in the string theory. For a quantum gravity system, the local quantum field cannot contain too many degrees of freedom, otherwise the formation of black hole is inevitable and then the quantum field theory breaks down. In the thermodynamics of the black hole [46, 47], there is a maximum entropy in a box of size L, namely the so-called Bekenstein entropy bound S_{BH}, which scales as the area of the box $\sim L^2$, rather than the volume $\sim L^3$. To avoid the breakdown of the local quantum field theory, Cohen *et al.* [48] proposed a more restrictive bound, i.e., the energy bound. If ρ_Λ is the quantum zero-point energy density caused by a short distance cut-off, the total energy in a box of size L cannot exceed the mass of a black hole of the same size [48], namely $L^3\rho_\Lambda \lesssim Lm_p^2$. The largest IR cut-off L is the one saturating the inequality. Thus,

$$\rho_\Lambda = 3c^2\, m_p^2\, L^{-2}, \tag{29}$$

where the numerical constant $3c^2$ is introduced for convenience. For the HDE model proposed in [49], the cut-off L has been chosen to be the future event horizon R_h, which is given by

$$R_h = a\int_t^\infty \frac{d\tilde{t}}{a} = a\int_a^\infty \frac{d\tilde{a}}{H\tilde{a}^2}\,. \tag{30}$$

From Eqs. (29), (30), and the energy conservation equation $\dot{\rho}_\Lambda + 3H\rho_\Lambda(1+w_\Lambda) = 0$, it is easy to find that (see e.g. [49–53])

$$\frac{d\Omega_\Lambda}{dz} = -(1+z)^{-1}\Omega_\Lambda(1-\Omega_\Lambda)\left(1+\frac{2}{c}\sqrt{\Omega_\Lambda}\right), \tag{31}$$

where Ω_Λ is the fractional energy density of HDE. From the Friedmann equation $H^2 = (\rho_m+\rho_\Lambda)\,/\,(3m_p^2)$, we have

$$E(z) = \left[\frac{\Omega_{m0}(1+z)^3}{1-\Omega_\Lambda(z)}\right]^{1/2}. \tag{32}$$

There are 2 independent model parameters, namely Ω_{m0} and c. One can obtain $\Omega_\Lambda(z)$ by solving the differential equation (31) with the initial condition $\Omega_\Lambda(z=0) = 1-\Omega_{m0}$. Substituting $\Omega_\Lambda(z)$ into Eq. (32), we can find the corresponding $E(z)$ and then the total χ^2 in Eq. (16). By minimizing the total χ^2, we find the best-fit parameters $\Omega_{m0} = 0.2764$ and $c = 0.7482$, while $\chi^2_{min} = 566.215$. In Fig. 9, we present the corresponding 68% and 95% confidence level contours in the $\Omega_{m0} - c$ parameter space for the HDE model.

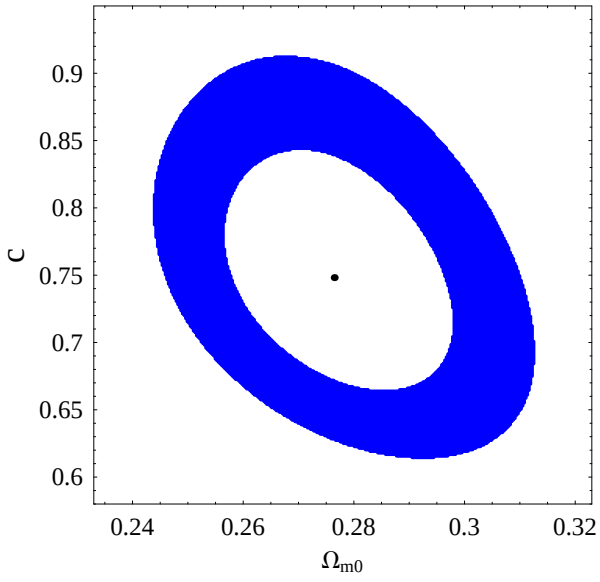

FIG. 9: The 68% and 95% confidence level contours in the $\Omega_{m0} - c$ parameter space for the HDE model. The best-fit parameters are also indicated by a black solid point.

E. Ricci dark energy model

The so-called Ricci dark energy (RDE) model was proposed in [54], which can be regarded as a variant of HDE mentioned above, while its corresponding cut-off L in Eq. (29) is chosen to be proportional to the Ricci scalar curvature radius. In [54], there is no physical motivation to this proposal for L in fact.

Recently, in [55] it is found that the Jeans length $R_{\rm CC}$ which is determined by $R_{\rm CC}^{-2}=\dot{H}+2H^2$ gives the causal connection scale of perturbations in the flat universe. Since the Ricci scalar is also proportional to $\dot{H}+2H^2$ in the flat universe, the physical motivation for RDE has been found in [55] actually. In the RDE model, the corresponding ρ_Λ is given by [54]

$$\rho_\Lambda=3\alpha m_p^2\left(\dot{H}+2H^2\right), \tag{33}$$

where α is a positive constant (when L is chosen to be $R_{\rm CC}$ in Eq. (29), one can see that $\alpha=c^2$ in fact). Substituting Eq. (33) into Friedmann equation, it is easy to find that [53, 54]

$$E(z)=\left[\frac{2\Omega_{m0}}{2-\alpha}(1+z)^3+\left(1-\frac{2\Omega_{m0}}{2-\alpha}\right)(1+z)^{4-2/\alpha}\right]^{1/2}. \tag{34}$$

There are 2 independent model parameters, namely Ω_{m0} and α. By minimizing the corresponding total χ^2 in Eq. (16), we find the best-fit parameters $\Omega_{m0}=0.3223$ and $\alpha=0.3559$, while $\chi^2_{min}=589.026$. In Fig. 10, we present the corresponding 68% and 95% confidence level contours in the $\Omega_{m0}-\alpha$ parameter space for the RDE model.

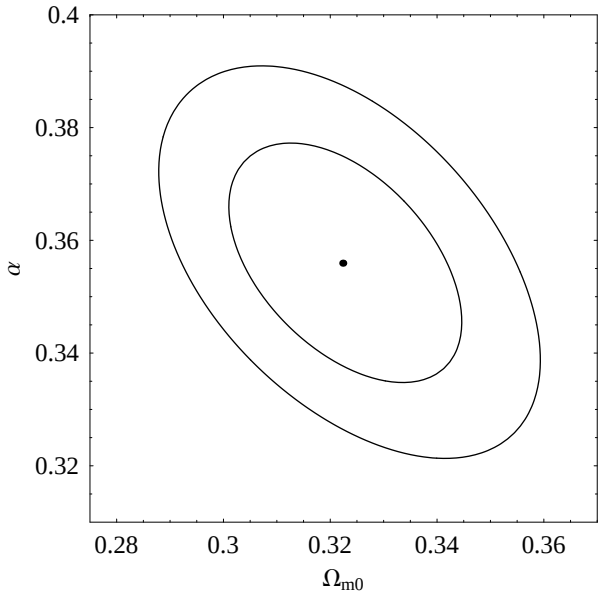

FIG. 10: The 68% and 95% confidence level contours in the $\Omega_{m0}-\alpha$ parameter space for the RDE model. The best-fit parameters are also indicated by a black solid point.

V. COMPARISON OF MODELS

In the previous section, we have obtained the constraints on 7 cosmological models with the latest observational data, namely, the combination of 557 Union2 SNIa dataset [20], 59 calibrated Hymnium GRBs dataset (obtained in this work), the shift parameter R from the WMAP7 data [21], and the distance parameter A of the measurement of the BAO peak in the distribution of SDSS luminous red galaxies [22, 23]. In Table III, we summarize the results for these 7 models. Here, we would like to briefly consider the comparison of these models. Naively, one can compare them with their χ^2_{min}, i.e., the best model has the smallest χ^2_{min} (vice versa). However, as is well known, in general χ^2_{min} decreases when the number of free model parameters increases. So, χ^2_{min} is not a good criterion for model comparison. Instead, a conventional criterion for model comparison in the literature is χ^2_{min}/dof, in which the degree

Model	ΛCDM	XCDM	CPL	DGP	NADE	HDE	RDE
χ^2_{min}	566.173	566.168	566.007	611.794	594.449	566.215	589.026
k	1	2	3	1	1	2	2
χ^2_{min}/dof	0.918	0.919	0.920	0.992	0.963	0.919	0.956
ΔBIC	0	6.421	12.687	45.621	28.276	6.468	29.280
ΔAIC	0	1.995	3.834	45.621	28.276	2.042	24.853
Rank	1	$2\sim3$	4	7	$5\sim6$	$2\sim3$	$5\sim6$

TABLE III: Summarizing all the 7 models considered in this work.

of freedom $dof = N - k$, whereas N and k are the number of data points and the number of free model parameters, respectively. We present the χ^2_{min}/dof for all the 7 models in Table III. On the other hand, there are other criterions for model comparison in the literature. The most sophisticated criterion is the Bayesian evidence (see e.g. [56] and references therein). However, the computation of Bayesian evidence usually consumes a large amount of time and power. As an alternative, one can consider some approximations of Bayesian evidence, such as the so-called Bayesian Information Criterion (BIC) and Akaike Information Criterion (AIC). The BIC is defined by [57]

$$\mathrm{BIC} = -2\ln\mathcal{L}_{max} + k\ln N\,, \tag{35}$$

where $\mathcal{L}_{max}$ is the maximum likelihood. In the Gaussian cases, $\chi^2_{min} = -2\ln\mathcal{L}_{max}$. So, the difference in BIC between two models is given by $\Delta\mathrm{BIC} = \Delta\chi^2_{min} + \Delta k\ln N$. The AIC is defined by [58]

$$\mathrm{AIC} = -2\ln\mathcal{L}_{max} + 2k\,. \tag{36}$$

The difference in AIC between two models is given by $\Delta\mathrm{AIC} = \Delta\chi^2_{min} + 2\Delta k$. We refer to e.g. [52, 59] for some relevant works with BIC and AIC. In Table III, we also present the ΔBIC and ΔAIC of all the 7 models considered in this work. Notice that ΛCDM has been chosen to be the fiducial model when we calculate ΔBIC and ΔAIC. From Table III, it is easy to see that the rank of models is coincident in all the 3 criterions (χ^2_{min}/dof, BIC and AIC). The ΛCDM model is still the best one, whereas DGP model is the worst one. The detailed rank of all the 7 models is also given in Table III.

VI. CONCLUSIONS

In the present work, by the help of the newly released Union2 compilation which consists of 557 SNIa, we calibrated 109 long GRBs with the well-known Amati relation, using the cosmology-independent calibration method proposed in [12]. We have obtained 59 calibrated high-redshift GRBs which can be used to constrain cosmological models without the circularity problem (we call them Hymnium GRBs sample for convenience). One can directly read off the numerical data of these 59 Hymnium GRBs from Table II of this paper. They are also available upon request to our email address. Considering their unique ability to extend our vision up to redshift $z = 8.1$, we recommend to use these 59 Hymnium GRBs in the relevant works.

We considered the joint constraints on 7 cosmological models from the latest observational data, namely, the combination of 557 Union2 SNIa dataset [20], 59 calibrated Hymnium GRBs dataset (obtained in this work), the shift parameter R from the WMAP7 data [21], and the distance parameter A of the measurement of the BAO peak in the distribution of SDSS luminous red galaxies [22, 23]. Note that in general it is better to see how the parameters are constrained both with and without GRBs. However, in fact the cosmological constraints on the same models without GRBs have been considered in e.g. [52], although they used slightly earlier SNIa and CMB data. So, we do not consider the constraints without GRBs in the present work. Comparing with the previous results in the literature (e.g. [52]), one can find that the constraints obtained in this work are tighter, thanks to these newly improved observational data. We also briefly considered the comparison of these 7 cosmological models. The ΛCDM model is still the best one from the perspective of the latest cosmological observations.

ACKNOWLEDGEMENTS

We thank the anonymous referee for quite useful comments and suggestions, which help us to improve this work. We are indebted to Lorenzo Amati for providing us the data of 14 unpublished GRBs in private communication and kindly allowing us to use them in our relevant works. We are grateful to Professors Rong-Gen Cai and Shuang Nan Zhang for helpful discussions. We also thank Minzi Feng, as well as Xiao-Peng Ma and Bo Tang, for kind help and discussions. This work was supported in part by NSFC under Grant No. 10905005, the Excellent Young Scholars Research Fund of Beijing Institute of Technology, and the Fundamental Research Fund of Beijing Institute of Technology.

---

[1] E. J. Copeland, M. Sami and S. Tsujikawa, Int. J. Mod. Phys. D **15**, 1753 (2006) [hep-th/0603057];
J. Frieman, M. Turner and D. Huterer, Ann. Rev. Astron. Astrophys. **46**, 385 (2008) [arXiv:0803.0982];
S. Tsujikawa, arXiv:1004.1493 [astro-ph.CO].
[2] B. E. Schaefer, Astrophys. J. **660**, 16 (2007) [astro-ph/0612285].
[3] V. Bromm and A. Loeb, Astrophys. J. **575**, 111 (2002) [astro-ph/0201400];
J. R. Lin, S. N. Zhang and T. P. Li, Astrophys. J. **605**, 819 (2004) [astro-ph/0311363].
[4] G. Ghirlanda, G. Ghisellini and C. Firmani, New J. Phys. **8**, 123 (2006) [astro-ph/0610248].
[5] B. Zhang, Chin. J. Astron. Astrophys. **7**, 1 (2007) [astro-ph/0701520];
B. Zhang, astro-ph/0611774.
[6] P. Meszaros, Rept. Prog. Phys. **69**, 2259 (2006) [astro-ph/0605208];
V. Bromm and A. Loeb, arXiv:0706.2445 [astro-ph];
S. E. Woosley and J. S. Bloom, Ann. Rev. Astron. Astrophys. **44** (2006) 507 [astro-ph/0609142].
[7] G. Ghirlanda, G. Ghisellini and C. Firmani, New J. Phys. **8**, 123 (2006) [astro-ph/0610248].
[8] G. Ghirlanda, G. Ghisellini, D. Lazzati and C. Firmani, Astrophys. J. **613**, L13 (2004) [astro-ph/0408350].
[9] C. Firmani *et al.*, Mon. Not. Roy. Astron. Soc. **360**, L1 (2005) [astro-ph/0501395].
[10] H. Li *et al.*, Astrophys. J. **680**, 92 (2008) [arXiv:0711.1792].
[11] E. W. Liang and B. Zhang, Mon. Not. Roy. Astron. Soc. **369**, L37 (2006) [astro-ph/0512177].
[12] N. Liang, W. K. Xiao, Y. Liu and S. N. Zhang, Astrophys. J. **685**, 354 (2008) [arXiv:0802.4262].
[13] Y. Kodama *et al.*, Mon. Not. Roy. Astron. Soc. **391**, L1 (2008) [arXiv:0802.3428].
[14] N. Liang and S. N. Zhang, AIP Conf. Proc. **1065**, 367 (2008) [arXiv:0808.2655];
T. S. Wang and N. Liang, arXiv:0910.5835 [astro-ph.CO];
N. Liang, P. Wu and S. N. Zhang, Phys. Rev. D **81**, 083518 (2010) [arXiv:0911.5644];
H. Gao, N. Liang and Z. H. Zhu, arXiv:1003.5755 [astro-ph.CO].
[15] H. Wei and S. N. Zhang, Eur. Phys. J. C **63**, 139 (2009) [arXiv:0808.2240].
[16] L. Amati *et al.*, Mon. Not. Roy. Astron. Soc. **391**, 577 (2008) [arXiv:0805.0377].
[17] L. Amati, arXiv:1002.2232 [astro-ph.HE].
[18] L. Amati, F. Frontera and C. Guidorzi, arXiv:0907.0384 [astro-ph.HE].
[19] We are grateful to L. Amati for providing us the numerical data of 14 unpublished GRBs in private communication and kindly allowing us to use them in our relevant papers. Note that there is an additional GRB 091024 beyond the 13 GRBs mentiond in [17].
[20] R. Amanullah *et al.* [Supernova Cosmology Project Collaboration], arXiv:1004.1711 [astro-ph.CO].
The numerical data of the full Union2 sample are available at http://supernova.lbl.gov/Union
[21] E. Komatsu *et al.* [WMAP Collaboration], arXiv:1001.4538 [astro-ph.CO].
[22] M. Tegmark *et al.* [SDSS Collaboration], Phys. Rev. D **69**, 103501 (2004) [astro-ph/0310723];
M. Tegmark *et al.* [SDSS Collaboration], Astrophys. J. **606**, 702 (2004) [astro-ph/0310725];
U. Seljak *et al.* [SDSS Collaboration], Phys. Rev. D **71**, 103515 (2005) [astro-ph/0407372];
M. Tegmark *et al.* [SDSS Collaboration], Phys. Rev. D **74**, 123507 (2006) [astro-ph/0608632].
[23] D. J. Eisenstein *et al.* [SDSS Collaboration], Astrophys. J. **633**, 560 (2005) [astro-ph/0501171].
[24] L. Amati *et al.*, Astron. Astrophys. **390**, 81 (2002) [astro-ph/0205230].
[25] L. Amati, Mon. Not. Roy. Astron. Soc. **372**, 233 (2006) [astro-ph/0601553].
[26] D. Eichler and A. Levinson, Astrophys. J. **614**, L13 (2004) [astro-ph/0405014];
A. Levinson and D. Eichler, Astrophys. J. **629**, L13 (2005) [astro-ph/0504125].

[27] R. Yamazaki, K. Ioka and T. Nakamura, Astrophys. J. **606**, L33 (2004) [astro-ph/0401044];
K. Toma, R. Yamazaki and T. Nakamura, Astrophys. J. **635**, 481 (2005) [astro-ph/0504624].
[28] M. J. Rees and P. Meszaros, Astrophys. J. **628**, 847 (2005) [astro-ph/0412702].
[29] T. Isobe, E. D. Feigelson, M. G. Akritas and G. J. Babu, Astrophys. J. **364**, 104 (1990).
[30] S. Nesseris and L. Perivolaropoulos, Phys. Rev. D **72**, 123519 (2005) [astro-ph/0511040];
L. Perivolaropoulos, Phys. Rev. D **71**, 063503 (2005) [astro-ph/0412308].
[31] E. Di Pietro and J. F. Claeskens, Mon. Not. Roy. Astron. Soc. **341**, 1299 (2003) [astro-ph/0207332].
[32] Y. Wang and P. Mukherjee, Astrophys. J. **650**, 1 (2006) [astro-ph/0604051].
[33] J. R. Bond, G. Efstathiou and M. Tegmark, Mon. Not. Roy. Astron. Soc. **291**, L33 (1997) [astro-ph/9702100].
[34] S. Nesseris and L. Perivolaropoulos, Phys. Rev. D **70**, 043531 (2004) [astro-ph/0401556].
[35] M. Chevallier and D. Polarski, Int. J. Mod. Phys. D **10**, 213 (2001) [gr-qc/0009008];
E. V. Linder, Phys. Rev. Lett. **90**, 091301 (2003) [astro-ph/0208512].
[36] R. Lazkoz, S. Nesseris and L. Perivolaropoulos, JCAP **0511**, 010 (2005) [astro-ph/0503230].
[37] H. Wei, N. N. Tang and S. N. Zhang, Phys. Rev. D **75**, 043009 (2007) [astro-ph/0612746].
[38] G. R. Dvali, G. Gabadadze and M. Porrati, Phys. Lett. B **485**, 208 (2000) [hep-th/0005016].
[39] C. Deffayet, Phys. Lett. B **502**, 199 (2001) [hep-th/0010186];
C. Deffayet, G. R. Dvali and G. Gabadadze, Phys. Rev. D **65**, 044023 (2002) [astro-ph/0105068].
[40] A. Lue, Phys. Rept. **423**, 1 (2006) [astro-ph/0510068].
[41] H. Wei, Phys. Lett. B **664**, 1 (2008) [arXiv:0802.4122].
[42] H. Wei and R. G. Cai, Phys. Lett. B **663**, 1 (2008) [arXiv:0708.1894].
[43] H. Wei and R. G. Cai, Phys. Lett. B **660**, 113 (2008) [arXiv:0708.0884].
[44] G. 't Hooft, gr-qc/9310026;
L. Susskind, J. Math. Phys. **36**, 6377 (1995) [hep-th/9409089].
[45] R. Bousso, Rev. Mod. Phys. **74**, 825 (2002) [hep-th/0203101].
[46] J. D. Bekenstein, Phys. Rev. D **7** (1973) 2333;
J. D. Bekenstein, Phys. Rev. D **9**, 3292 (1974);
J. D. Bekenstein, Phys. Rev. D **23**, 287 (1981);
J. D. Bekenstein, Phys. Rev. D **49**, 1912 (1994) [gr-qc/9307035].
[47] S. W. Hawking, Commun. Math. Phys. **43**, 199 (1975) [Erratum-ibid. **46**, 206 (1976)];
S. W. Hawking, Phys. Rev. D **13**, 191 (1976).
[48] A. G. Cohen, D. B. Kaplan and A. E. Nelson, Phys. Rev. Lett. **82**, 4971 (1999) [hep-th/9803132].
[49] M. Li, Phys. Lett. B **603**, 1 (2004) [hep-th/0403127].
[50] X. Zhang and F. Q. Wu, Phys. Rev. D **76**, 023502 (2007) [astro-ph/0701405].
[51] H. Wei and S. N. Zhang, Phys. Rev. D **76**, 063003 (2007) [arXiv:0707.2129].
[52] M. Li, X. D. Li and X. Zhang, arXiv:0912.3988v1 [astro-ph.CO].
[53] M. Li, X. D. Li, S. Wang and X. Zhang, JCAP **0906**, 036 (2009) [arXiv:0904.0928].
[54] C. Gao, X. Chen and Y. G. Shen, Phys. Rev. D **79**, 043511 (2009) [arXiv:0712.1394].
[55] R. G. Cai, B. Hu and Y. Zhang, Commun. Theor. Phys. **51**, 954 (2009) [arXiv:0812.4504].
[56] A. R. Liddle, Mon. Not. Roy. Astron. Soc. **377**, L74 (2007) [astro-ph/0701113];
A. R. Liddle, Ann. Rev. Nucl. Part. Sci. **59**, 95 (2009) [arXiv:0903.4210].
[57] G. Schwarz, Ann. Stat. **6**, 461 (1978).
[58] H. Akaike, IEEE Trans. Automatic Control **19**, 716 (1974).
[59] W. Godlowski and M. Szydlowski, Phys. Lett. B **623**, 10 (2005) [astro-ph/0507322];
M. Szydlowski and W. Godlowski, Phys. Lett. B **633**, 427 (2006) [astro-ph/0509415];
M. Szydlowski, A. Kurek and A. Krawiec, Phys. Lett. B **642**, 171 (2006) [astro-ph/0604327];
M. Szydlowski, W. Godlowski and T. Stachowiak, Phys. Rev. D **77**, 043530 (2008) [arXiv:0706.0283];
M. Szydlowski and A. Kurek, arXiv:0801.0638 [astro-ph].
[60] In fact, up to now, there are more than 109 long GRBs with known redshifts and spectra peak energy, see e.g. [61] and references therein. However, since the numerical data of $E_{\rm p,i}$ and $S_{\rm bolo}$ are explicitly given in [17] (and [16, 18, 19]) which are more convenient for our computing, we choose to use these 109 long GRBs instead. One can easily extend our work with a larger GRBs sample.
[61] N. R. Butler, D. Kocevski, J. S. Bloom and J. L. Curtis, Astrophys. J. **671**, 656 (2007) [arXiv:0706.1275];
N. R. Butler, J. S. Bloom and D. Poznanski, Astrophys. J. **711**, 495 (2010) [arXiv:0910.3341].
[62] N. M. Lloyd, V. Petrosian and R. S. Mallozzi, Astrophys. J. **534**, 227 (2000) [astro-ph/9908191].
[63] We thank the the anonymous referee for pointing out this issue.

[64] E. Nakar and T. Piran, Mon. Not. Roy. Astron. Soc. **360**, 73 (2005) [astro-ph/0412232];
D. L. Band and R. D. Preece, Astrophys. J. **627**, 319 (2005) [astro-ph/0501559];
A. S. Friedman and J. S. Bloom, Astrophys. J. **627**, 1 (2005) [astro-ph/0408413];
N. R. Butler, D. Kocevski and J. S. Bloom, Astrophys. J. **694**, 76 (2009) [arXiv:0802.3396];
A. Shahmoradi and R. J. Nemiroff, arXiv:0904.1464 [astro-ph.HE].
[65] S. Basilakos and L. Perivolaropoulos, Mon. Not. Roy. Astron. Soc. **391**, 411 (2008) [arXiv:0805.0875].
[66] H. Wei, Phys. Lett. B **691**, 173 (2010) [arXiv:1004.0492];
H. Wei, Phys. Lett. B **692**, 167 (2010) [arXiv:1005.1445].